Research Article Vol. 60, No. 4 / 1 February 2021 / Applied Optics 1051

applied optics

Concentration and pressure scaling of CH_2O electronic-resonance-enhanced coherent anti-Stokes Raman scattering signals

Daniel K. Lauriola,[1] K. Arafat Rahman,[1] Hans U. Stauffer,[2] Mikhail N. Slipchenko,[1,2] Terrence R. Meyer,[1] and Sukesh Roy[2,*]

[1]Purdue University, School of Mechanical Engineering, West Lafayette, Indiana 47907, USA
[2]Spectral Energies, LLC, 4065 Executive Dr., Beavercreek, Ohio 45430, USA
*Corresponding author: sukesh.roy@spectralenergies.com

Received 20 November 2020; revised 29 December 2020; accepted 30 December 2020; posted 5 January 2021 (Doc. ID 415496); published 28 January 2021

Nanosecond electronic-resonance-enhanced coherent anti-Stokes Raman scattering (ERE-CARS) is evaluated for the measurement of formaldehyde (CH_2O) concentrations in reacting and nonreacting conditions. The three-color scheme utilizes a 532 nm pump beam and a scanned Stokes beam near 624 nm for Raman excitation of the C–H symmetric stretch (ν_1) vibrational mode; further, a 342 nm resonant probe is tuned to produce the outgoing CARS signal via the $1_0^1 4_0^3$ vibronic transition between the ground ($\tilde{X}^1A_1$) and first excited ($\tilde{A}^1A_2$) electronic states. This allows detection of CH_2O at concentrations as low as 9×10^{14} molecules/cm^3 (55 parts per million) in a calibration cell with CH_2O and N_2 at 1 bar and 450 K with 3% uncertainty. The measurements show a quadratic dependence of the signal with CH_2O number density. Pressure scaling experiments up to 11 bar in the calibration cell show an increase in signal up to 8 bar. We study pressure dependence up to 11 bar and further apply the technique to characterize the CH_2O concentration in an atmospheric premixed dimethyl ether/air McKenna burner flame, with a maximum concentration uncertainty of 11%. This approach demonstrates the feasibility for spatially resolved measurements of minor species such as CH_2O in reactive environments and shows promise for application in high-pressure combustors.

https://doi.org/10.1364/AO.415496

1. INTRODUCTION

The accurate measurement of minor-species concentrations, such as that of formaldehyde (CH_2O), is necessary for emissions monitoring and can play a key role in understanding the thermochemistry of various combustion processes [1,2]. Because formaldehyde is a known carcinogen and pollutant, it is important to measure atmospheric CH_2O with parts per million (ppm) sensitivity [3]. In combustion, formaldehyde is an important intermediate for the oxidation of hydrocarbons. It is used to detect the presence of cool flames [4], visualize flame fronts [5], measure ignition delay [6], and provide modeling insight into numerous intermediate chemical reactions [7]. As such, background-free, spatially resolved measurements of ppm levels of formaldehyde in reactive and nonreactive environments are of fundamental and practical interest. Additionally, formaldehyde is one of the simplest asymmetric top molecules, representing a benchmark for more complex molecules.

Various experimental techniques have been applied in the gas phase to either confirm the molecular structure or provide information to combustion models for the oxidation of CH_2O. Absorption spectroscopy (AS) and four-wave mixing have been employed to investigate the rotational structure of the electronic ground [8,9] and excited states [10–12], while Fourier transform infrared spectroscopy (FTIR) has been used to measure CH_2O concentrations in gas samples collected from a dimethyl ether (DME) flame [13].

CH_2O planar laser-induced fluorescence (PLIF) has allowed determination of the 2D distribution of formaldehyde in applications such as turbulent flames [14–19], high-pressure environments [20], across shock waves [21], and to mark the ignition zone in a scramjet engine. Demonstration of qualitative CH_2O PLIF has been accomplished at repetition rates as high as 100 kHz [22], and the intensity change in the PLIF signal has also been used as a semiquantitative technique in DME flames [6]. Many of the described techniques for measuring concentration suffer from spatial resolution limitations, line-of-sight averaging (AS [8,10], FTIR [13]), or sensitivities to the molecular quenching environment (PLIF [15,17–21]).

Spatially resolved, quantitative background-free measurements of many combustion species over varying pressures have been made possible by coherent anti-Stokes Raman scattering spectroscopy (CARS). CARS is a nonlinear optical technique

that targets transitions of vibrational or rotational energy states of a polarizable medium using the frequency difference between two electric fields (pump and Stokes). The Raman resonances that exist near the pump/Stokes difference frequencies are subsequently probed by a third electric field (probe). The method is widely used in combustion because it allows for excellent spatial resolution and can be background-free with the appropriate experimental arrangement. Variations of CARS have been widely used for temperature and major-species concentration measurements [23]. Recently, femtosecond CARS [24] has been used to study the rotational structure of the S_0 ($\tilde{X}^1A_1$) ground electronic state at 80 mbar and to improve accuracy of Raman spectral modeling of CH_2O, where Coriolis interactions between different levels affect the strength and position of lines in the ground electronic state ν_1 (symmetric C–H stretch) vibrational level near 2782 cm^{-1}.

As CARS signals scale quadratically with the absolute number density of the probed molecule, measurements can be limited to chemical species with relatively high concentrations. For low-concentration measurements in a combustion environment, electronic-resonance-enhanced (ERE) CARS has been shown to be a promising technique [25]. In this variation of CARS, one or more of the laser wavelengths is tuned to access an electronic resonance of the molecule. Coupling the pump or probe beams to an electronic level, instead of to a virtual state, can increase the signal level a thousand-fold, enabling ppm-level detection. ERE-CARS has already been demonstrated as a spatially resolved technique in a flame for the detection of NO [26,27], C_2 [25], and OH. Attal-Trétout *et al.* [28] measured the OH concentration in a high-pressure environment, and Wrzesinski *et al.* [29] used femtosecond fully resonant electronically enhanced CARS (FREE-CARS) of OH for simultaneous flame temperature and concentration measurements.

In this work, we demonstrate ERE-CARS of CH_2O, allowing quantitative concentration measurements at low ppm mole fractions in both reacting and nonreacting environments. Access to the Raman-active fundamental transition of the ν_1 band of the ground S_0 electronic level of CH_2O is achieved by tuning the Stokes beam wavelength (~624 nm) relative to a fixed pump wavelength (532 nm), whereas electronic enhancement results from a UV probe wavelength (~342 nm) that couples these states to the (1,0,0,3,0,0) vibronic band of the first singlet S_1 ($\tilde{A}^1A_2$) excited state [Fig. 1(a)], producing an outgoing CARS signal (~312 nm) via $1_0^1 4_0^3$ vibronic transitions. Using this optical setup, we have characterized the pressure and concentration scaling of the CH_2O ERE-CARS signals in a nonreacting mixture with N_2. Application of this technique toward concentration measurements of CH_2O was subsequently demonstrated in a premixed dimethyl ether (DME)/air flame stabilized over a McKenna burner at atmospheric pressure.

2. EXPERIMENTAL APPARATUS

As shown in Fig. 1(b), the experimental setup employed an injection-seeded Nd:YAG laser (Spectra Physics, GCR-3) providing 700 mJ/pulse second-harmonic (532 nm) output at 10 Hz; the spectral linewidth (full width at half maximum, FWHM) of this output was measured (HighFinesse WS7

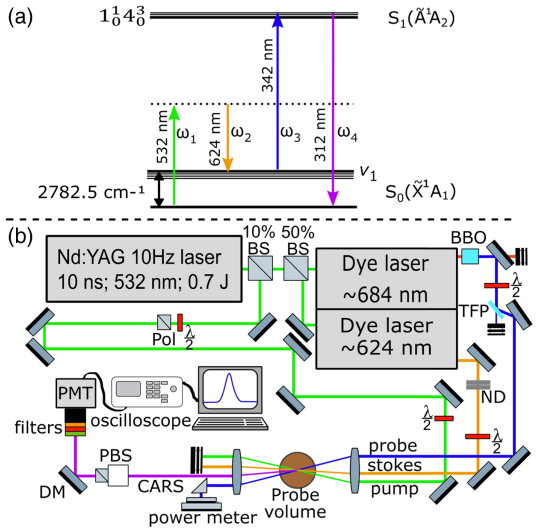

Fig. 1. (a) Formaldehyde energy-level diagram. The fundamental ν_1 vibrational band of ground state (S_0)CH_2O was probed; probe resonance with the excited electronic state (S_1) was used for signal enhancement. (b) Three beam ERE-CARS setup. BS, beam splitter; Pol, polarizer; ND, neutral density filter; BBO, beta barium borate crystal; TFP, thin film polarizer; DM, dichroic mirror; $\lambda/2$, half-wave plate; PBS, α−BBO polarizing beam splitter. At the probe volume, either a nonreacting pressure vessel or a premixed flat flame stabilized McKenna burner was used.

wave meter) to be 0.02 cm^{-1}. The 532 nm pump beam in the ERE-CARS scheme was produced by splitting off 10% of this output energy; the remaining was subsequently split with a 50/50 beam splitter to pump two narrowband single-grating dye lasers (Continuum, ND6000). In the first dye laser, a mixture of DCM dye (exciton) and ethanol was used to produce a 50 mJ/pulse Stokes beam, (15% conversion efficiency), tunable from 15,966 to 16,052 cm^{-1} (~623−626.3 nm), with a measured linewidth (FWHM) of 0.1 cm^{-1} and <10% pulse-to-pulse energy variation. In the second dye laser, LD688 dye (exciton) and methanol were mixed to generate output that was subsequently frequency-doubled in a Type-I β-barium borate (β−BBO) crystal to produce the probe beam, tunable from 29,200 to 29,450 cm^{-1} (~339.6−342.5 nm), with a measured linewidth of 0.2 cm^{-1} (FWHM), and UV energy of 17 mJ/pulse (5% 532 to 342 nm conversion). The wavelengths and energies at each step were recorded during the experiment for use in post-processing of the measured ERE-CARS spectra.

Per-pulse energy adjustment of the pump and probe beams was performed using half-wave plate (HWP) and polarizer combinations, whereas neutral density filters were used for attenuation of the Stokes beam. For the experiments in the pressure vessel, the beams were all vertically polarized. However, for experiments in the McKenna burner, polarization-based nonresonant background suppression was necessary. This was accomplished by setting the pump and Stokes polarizations at 60° with respect to vertical, and an α−BBO polarizing beam splitter on the detection side was set to 30°, perpendicular to the nonresonant background signal. This polarization configuration produced a 10^4 attenuation of the nonresonant background while incurring only a tenfold loss in the resonant signal [25,30].

The beams were directed into the probe volume in a folded BOXCARS arrangement [31]. The incoming beams were focused, and the outgoing ERE-CARS signal subsequently recollimated using 150 mm focal length plano-convex lenses (UV-grade fused silica). On the output, a physical mask was used to block the pump and Stokes beams, and the probe beam was directed into an energy monitor. The CARS signal beam was reflected by a 45° high reflector at 312 nm into three 310 nm bandpass filters (Edmund Optics, 34976, 10 nm FWHM) and a UV short-pass filter (Thorlabs, FGUV11M) to eliminate any stray scattering of the input beams before being measured by a UV sensitive photomultiplier tube (Hamamatsu R9110). The photomultiplier tube was connected to an oscilloscope (Rigol, 1000Z), controlled by a LabVIEW VI, used to save single-shot or averaged traces to the computer for post-processing analysis. A typical scan, depending on the range and resolution, lasted 10 to 25 min, as 64 laser shots were averaged for each step.

An optically accessible mixing chamber rated up to 30 bar with four 0.25-in.-thick UV-fused silica windows was used for conducting high-pressure experiments in an N_2 and CH_2O mixture. The mole fractions of N_2 and CH_2O were set by the following procedure, similar to that used by Walser *et al.* [32,33]: a 37% CH_2O aqueous solution (Fischer Scientific) was first placed in a windowless stainless-steel evaporation chamber; the evaporation chamber was heated to 475 K with heating tape, and the pressure vessel was evacuated and heated to 450 K; after 20 min, the valve between the chambers was opened, and the gas passed through a colder section to condense out some of the water before entering the windowed vessel; after a few minutes, the test chamber was again isolated from the evaporation chamber with a manual valve; heated N_2 was then slowly added from a separate port to attain the desired pressure. As previously reported in [10,32], every time the vessel was cooled down to room temperature, a white film of polymerized CH_2O formed on the inner walls, requiring cleaning. To avoid polymerization, the pressure vessel was covered by heat tape, and hot air jets were directed at the windows. This system was designed to mix CH_2O in an N_2 environment with a mole fraction as low as 55 ppm at 1 bar. The uncertainty in the mixture fraction of CH_2O was approximately 5% at pressures from 0.5 to 11 bar, and the temperature was set at 450 K for the experiments in the pressure vessel. For experiments with the DME/air flame, a flat-flame porous plug McKenna burner, analogous to the one described in [13], replaced the pressure vessel.

Saturation of the CARS signal as a function of the energy of each of the CARS beams was measured, and it was found that the energy in the pump and Stokes beams must remain under 10 mJ/pulse, whereas the probe energy must be under 2 mJ/pulse, to avoid saturation. During the experiments in the pressure vessel, energies for each beam were kept at or below 3 mJ/pulse to avoid damage to the window and corresponding degradation of the input beams.

3. RESULTS AND DISCUSSION

A. Mixing Chamber Calibration

Characterization of the spectral response of the ERE-CARS signal was performed by scanning either the Stokes or probe frequencies during measurements of CH_2O in N_2 (mole fraction = 700 ppm) at 450 K and 1 bar in the pressure vessel described in the experimental setup. Initially, the Stokes-beam frequency was fixed to access the fundamental ν_1 band head at a Raman shift of 2782.5 cm^{-1} [34], while the probe frequency was scanned from 29,230 to 29,300 cm^{-1} (step size of 0.2 cm^{-1}). An average of two probe-frequency scans is shown in Fig. 2(a), performed with a pump and Stokes energy of 2 and 3 mJ/pulse, respectively, and a wavelength-dependent probe energy between 0.3 and 1 mJ/pulse. The results have been corrected for probe-pulse intensity variance with wavelength. This scan in Fig. 2(a), therefore, shows the wavelength dependence associated with electronic resonance enhancement of CARS signal via the $1_1^1 4_0^3$ vibronic transition. Prior ERE-CARS experiments with NO have demonstrated broad resonance enhancement, with peaks spaced about 40 cm^{-1} [26], while for 2O, we observed two close separate peaks in the electronic resonance enhancement. Although the $1_1^1 4_0^3$ transition band of CH_2O has not been explicitly studied previously, these excitation features are consistent with comparable features observed in high-resolution scans of the $1_0^1 4_0^3$ absorption band, where two close distinct peaks were present at the transitions corresponding to the outgoing CARS signal of the probe scan [10]. While direct absorption might not take into account the resonant features of the ERE-CARS interaction, higher-resolution measurements of CH_2O performed using FREE-CARS in our laboratory (not shown here) also exhibit two well-resolved, strongly resonant ro-vibronic peaks ~20 cm^{-1} apart. While the probe scan range was limited here by the probe dye laser wavelength range, excitation scans by Bouwens *et al.* [35] as well as CH_2O FREE-CARS excitation-wavelength scans suggest that significantly stronger resonance enhancement might be obtained by using a probe redshifted by ~200 cm^{-1}. Exploration of different electronic enhancements could be an interesting application for further studies if higher sensitivity is of interest.

Figure 2(b) shows scans of the Stokes beam with a probe wavelength fixed at 29,260 cm^{-1} and 29,272 cm^{-1}, respectively [see Fig. 2(a)], while the Stokes beam was scanned with a 0.05 cm^{-1} step from a Raman shift of 2770 cm^{-1} to 2790 cm^{-1}. The first scan, with probe at 29,260 cm^{-1}, was performed three times at the same CH_2O/N_2 conditions to measure a 3% uncertainty in the scan repeatability. The resulting locations of the K_a levels were in agreement with the Coriolis-shift perturbation model and experimental fs-CARS measurements presented by Walser *et al.* [24] as well as the Raman spectra by Magnotti *et al.* [36]. The higher-resolution scans of this experiment showed the wrapping of the band head predicted by Walser *et al.*, the overlap of the $K_a = 1$ and $K_a = 2$ levels as well as line-strength differences in scans performed at the two probe wavelengths. The difference in the two scans can be understood based on the energy levels diagram shown in Fig. 1(b). The ro-vibrational band reached in the S_1 excited electronic level depends on all three frequencies: $\omega_4 = \omega_1 - \omega_2 + \omega_3$. During the Stokes scans, ω_1 and ω_3 are held constant, and ω_2 is scanned through different $(\omega_1 - \omega_2)$ Raman shifts, causing ω_4 to change with ω_2. As this Raman shift is varied to access different intermediate transitions, the probe accesses different final transitions within the S_1 excited electronic level, and the outgoing signal intensity

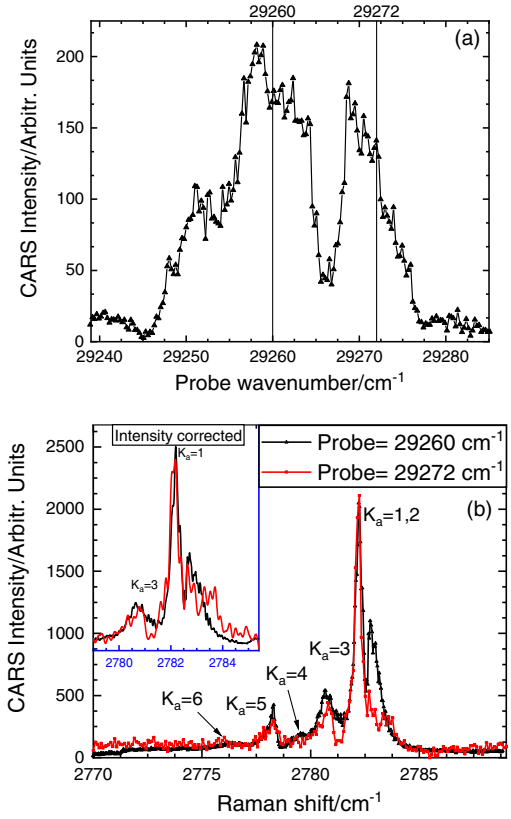

Fig. 2. Electronic-level splitting and its effect on the rotational levels of fundamental transition of the ν_1 vibrational mode. (a) Average of two wavelength scans of the probe beam at atmospheric pressure with 700 ppm of CH_2O in N_2 at 450 K. The Stokes beam was tuned to a Raman shift of 2782.5 cm^{-1} relative to the pump beam, and the probe beam was scanned in steps of 0.2 cm^{-1}. Each point was averaged over 64 laser shots. (b) Signal from wavelength scans of the Stokes beam for two different denoted probe frequencies tuned within the electronic resonance band. Scans were performed with a step size of 0.05 cm^{-1} and 64 shot average for each step. Inset in (b) shows a detail of the scans divided by the resonance enhancement measured in (a).

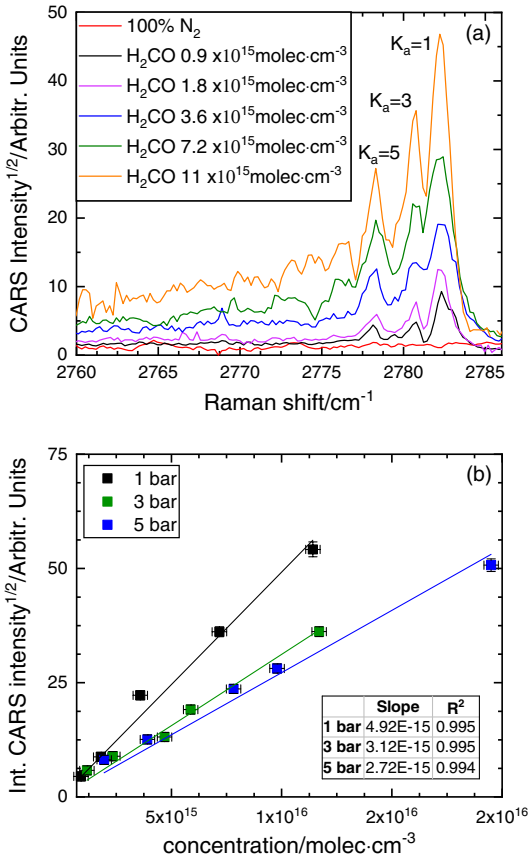

Fig. 3. (a) Scans performed at atmospheric pressure with increasing concentrations of CH_2O in N_2 to calibrate the technique for different concentrations and estimate a detectability limit. Scans were performed with a 0.2 cm^{-1} step size and 64-point averaging. (b) Concentration scaling at different pressures. The data points were obtained by integrating the intensity of the spectral scan from 2775 cm^{-1} to 2785 cm^{-1}. Solid lines represent the linear fits.

will depend on both the $(\omega_1 - \omega_2)$ intermediate levels as well as the transition probabilities into and out of the levels accessed by the probe, further complicating modeling of the spectra.

Direct comparison between the two scans was achieved via normalization of the spectra by the electronic resonance enhancement measured in Fig. 2(a): by knowing the initial probe and stokes frequencies, ω_4 was matched to map the probe scan onto the Stokes scans. The Stokes scan was then divided by the matched probe scan to normalize the resonance enhancement. This correction was applied to each scan in Fig. 2(b) [see inset Fig. 2(b)]. The electronic enhancement normalization worked for the $K_a = 3 - 5$ levels but did not completely match the band head ($K_a = 1, 2$), where the resonance probability appears to vary too significantly, as the resonance enhancement with the probe fixed at 29,272 cm^{-1} falls abruptly above 2782.5 cm^{-1}. Differences in the two scans may also result from different transition probabilities into S_1 for different Raman shifts. While outside the scope of this paper, multiple probe scans at different Raman shifts would be necessary to fully study the effects of the transition probabilities on the two scans.

The goal of the current experiment was to perform measurements in a region of constant electronic resonance, so the probe was set to the broadest of the two electronic transitions (29,260 cm^{-1}), providing sufficient enhancement for the range of Raman shifts from 2775 to 2784 cm^{-1} and with a rapid drop-off outside this range. This choice of the probe wavelength enabled measurements of the $K_a = 1 - 5$ transitions of the ν_1 vibrational band of the S_0 electronic level with little change in resonance, while higher K_a transitions remained outside of the maximum resonance enhancement and below the detection limit at atmospheric pressure.

The scaling of CH_2O ERE-CARS signal with concentration was performed in a mixture of CH_2O and N_2 at three different pressures. The probe laser was set to 29,260 cm^{-1}, and the Stokes dye laser scanned across a Raman Shift of 2760 to 2790 cm^{-1}, with a 0.2 cm^{-1} step size and 64-point averaging. The spectra shown in Fig. 3(a) were integrated between 2775 and 2785 cm^{-1} for each concentration. The square root of the result is plotted in Fig. 3(b), with a linear fit for each condition. At atmospheric pressure, a maximum signal-to-noise ratio (SNR) of 2,000 was achieved for a concentration of 1.14×10^{16} molecules/cm^3 of CH_2O (mole fraction of 700 ± 20 ppm, calculated from amount of CH_2O and N_2 pressure). An SNR

of 10 was achieved for the lowest measured concentration of 9×10^{14} molecules/cm^3 (mole fraction of 55 ± 20 ppm). The detection limit was estimated at 2×10^{14} molecules/cm^3 for an SNR of 1 (molar fraction of 12 ppm), although this concentration of CH_2O was too low to be accurately dispensed in the current system. As seen in Fig. 3(a), the nonresonant signal from 100% N_2 remained constant across the spectrum, which is much lower than the resonant signal.

The square root of the CARS signal intensity was found to be linear with number density, as observed previously in ERE-CARS experiments with other molecules [27], and can be inferred from theory, which predicts the intensity of CARS signal is proportional to the square of the number density [37]. The experiments for Fig. 3(b) were performed at constant pressures of 1, 3, and 5 bar, respectively, exhibiting a similar number density dependence. Above atmospheric pressure, the slope of the concentration scaling fit decreased, indicating that the effects of pressure may already have an influence from 3 bar. To test the influence of pressure on the concentration scaling, further experiments were performed in which the mole fraction of CH_2O was kept constant and the pressure was increased.

Figure 4(a) shows a sample of scans at pressures ranging from 1 to 11 bar. Each data point in Fig. 4(b) was calculated by integrating the spectra between 2775 and 2785 cm^{-1}, after nonresonant background subtraction, and shows two independent measurements. Figure 4(b) shows that, as pressure is increased, the signal does not follow the squared number density scaling. The signal increases slowly with pressure and flattens out above 8 bar. The deviation from the theoretically predicted squared number density dependence at high pressures was previously observed in ERE-CARS measurements of other species [23,38]. Absorption experiments at high pressure showed that up to 10% of the input 29,260 cm^{-1} probe beam energy was absorbed at 8 bar, but this is not enough to account for the flattening of the signal [39]. The deviation is likely caused by two factors: 1) collisional line broadening in both electronic levels; 2) reabsorption of the outgoing CARS beam. The indication of the line broadening associated with the final electronic transition is most obvious in the scan at 11 bar [Fig. 4(a)], in which higher excited $K_a = 7$ and 9 levels appear, suggesting that the electronic resonance has broadened sufficiently to bring transitions from these higher K_a states into resonance and plays a nontrivial role in the flattening of the signal. As the outgoing CARS signal wavelength matches the $1_0^1 4_0^3$ vibronic transition of CH_2O, reabsorption of the CARS signal through this same transition could also play a significant role in the signal flattening at higher pressures and number densities.

While further study of these effects is beyond the scope of this publication, the pressure scaling experiments show that the ERE-CARS technique can be used at least up to 11 bar and indicate that it is necessary to perform a constant pressure concentration calibration for the pressure expected during the experiment.

B. Application to Dimethyl Ether Flame

CH_2O ERE-CARS was tested in the reacting environment of an atmospheric pressure premixed DME/air flat-flame burner. This particular flame was selected because it could be compared

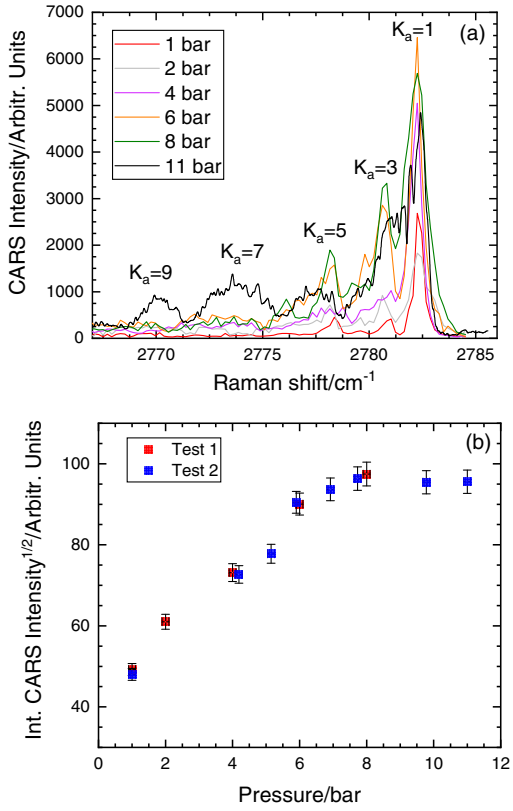

Fig. 4. (a) Stokes scans at a constant mole fraction of 700 ppm in N_2 and increasing pressures, which results in a linear number density increase with pressure. Scan step size of 0.2 cm^{-1} and 64 point averaging were used. The scan at 11 bar was performed with a 0.05 cm^{-1} step size. Pump, stokes, probe energies were set to 2, 3, and 0.5 mJ, respectively. (b) Square root of the integrated intensity under the curve between 2775 and 2785 cm^{-1} of the highest peak (~2782 cm^{-1}) after nonresonant background subtraction. Error bars in x of 0.1 bar and 3% in y. Test 1 and test 2 indicate scans performed on different days.

with the publication by Kaiser *et al.* [13] in which a thorough characterization of CH_2O concentration in a DME/air flame was performed using FTIR on gas samples extracted with a physical probe. The 25.4 mm diameter water-cooled McKenna flat-flame burner was mounted on a vertical translation stage, in place of the pressure vessel. Polarization-based nonresonant-background suppression was applied after experiments showed the nonresonant contribution of unburnt DME to be ~5% of the resonant signal. An image of the flame, the samples of three repeated Stokes scans in the DME flame at $\phi = 1.3$ and a calibration scan from the pressure vessel are shown in Fig. 5. The energies used for the flame were 6 mJ/pulse for the pump and Stokes beams and 1.5 mJ/pulse for the probe beam. Three scans were performed for each equivalence ratio; then, each data set was integrated from 2775 to 2785 cm^{-1} and calibrated with the integrated signal from the pressure vessel and the temperature-dependent number density of the flame. The standard deviation from multiple scans was used to estimate the uncertainty, which reached a maximum of 11% for the richest conditions ($\phi = 1.64$ and 2.19), where the flame also appeared unstable and likely contributed to increased signal fluctuations.

The vertical translation stage was moved from 0.25 to 1.75 mm above the burner with a 0.25 mm step, for a rich and

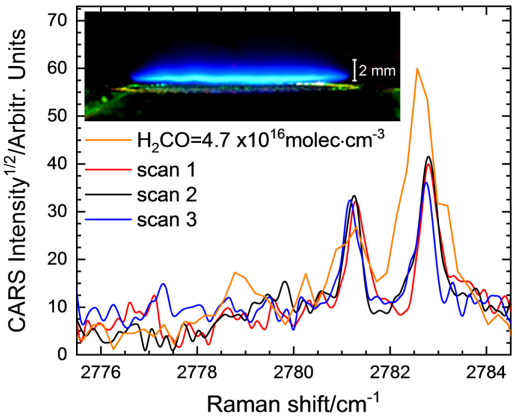

Fig. 5. Sample of three Stokes scans with a step size of 0.1 cm^{-1} at $\phi = 1.3$ and 0.75 mm above the burner surface. These scans were used to determine the uncertainty in the flame measurements, and the scan with $4.7 \cdot 10^{16}$ molec·cm^{-3} of CH_2O was performed in the pressure vessel for calibration. Inset: Image of the Mckenna burner flame at $\phi = 1.3$ with N_2 co-flow.

a lean flame condition [Fig. 6(a)]. The results were plotted with the physical probe sampling data from Kaiser *et al.* [13], with the stated ±10% precision. Both show an increase of CH_2O concentration in the premix zone and then a drop in the downstream, where the flame is hot and CH_2O is turned into reaction products. Downstream of the flame front the CH_2O concentration rapidly decays. For the $\phi = 0.67 \pm 0.05$ condition, the visible flame is much broader, and the change in CH_2O concentration is less pronounced in the upstream and in the downstream sides of the flame. Comparison of our results with the data from the physical probe experiments of Kaiser *et al.* [13] shows that the trends agree well in the pre-flame zone; however, after the flame front, our concentration measurements show a slower decay in the CH_2O concentration [see Fig. 6(a)]. The most apparent difference between the two experiments is that the ERE-CARS measurement is an *in situ* measurement, while in the previous method a sample is first extracted from the flame and then analyzed. It is possible that the probe quenched the flame, or that further reactions from CH_2O into products weren't interrupted quickly enough during the sampling. Small differences in the mass flows and in the absolute flame position are also probable and may explain the peak offset in the $\phi = 1.49$ condition. Overall, the general trends are in agreement for the two experiments.

Further experiments, as shown in Fig. 6(b), were performed by varying the equivalence ratio at a fixed height of 0.75 mm above the burner. The same experimental conditions of Fig. 6(a) were used, and the equivalence ratio was varied from 0.4 to 2.1. The specific height was selected because it is right before the flame front, where CH_2O oxidation should occur. Figure 6(b) shows a linear increase in CH_2O concentration in the oxidation layer up to a stochiometric flame, with a peak concentration around $\phi = 1.6$. As a comparison for these results could not be found in the literature, this measurement may be used as a guideline for modeling the CH_2O concentration in the oxidation layer of this nonadiabatic flame.

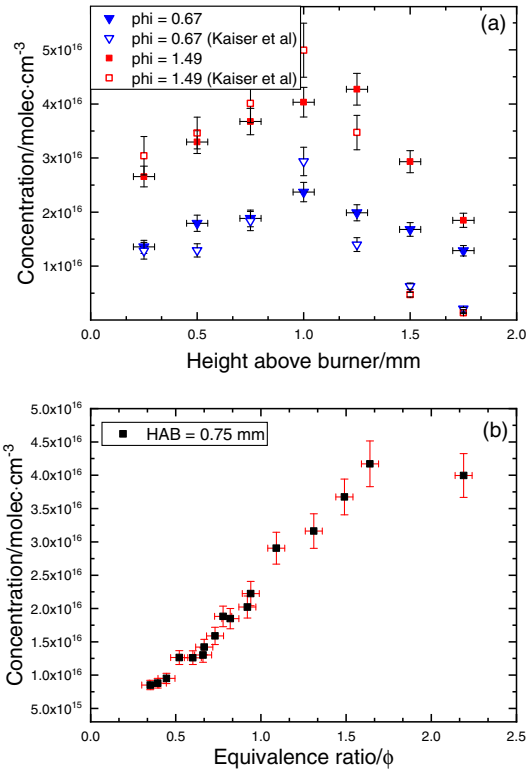

Fig. 6. (a) Concentration measurements for height scans at rich and lean flame conditions in a premixed DME/air McKenna burner. Concentration was obtained by integrating the signal from 2775 to 2785 cm^{-1}, calibrated with measurements in the pressure vessel. The height above the burner indicates the height of the probe volume above the top surface of the burner. The zero is set to where the probe volume hits the top surface of the burner. Y error bars are the standard deviation of multiple measurements, and x error bars represent the 0.05 mm uncertainty from the micrometer. Also shown are measurements by Kaiser *et al.* [13] in an analogous burner. (b) Concentration measurements of an equivalence ratio scan 0.75 mm above the burner. The x error bars represent ±0.05 uncertainty in the equivalence ratio, and the y error bars are from the standard deviation of multiple trials.

4. CONCLUSIONS

In this work, quantitative ERE-CARS measurements of the CH_2O concentration were performed in a high-pressure mixing chamber and in a premixed DME/air flat-flame. Characterization data showed two close transitions in the $1_1^1 4_0^3$ vibronic transition band that could each provide electronic enhancement of the CARS signal mediated by the Raman-active ν_1 vibrational band of the ground electronic state.

The measurements showed that the technique is effective at mole fractions lower than 55 parts per million of CH_2O in N_2 at 450 K, with an estimated detectability limit of 12 ppm. The quadratic dependence of the signal on the concentration was in agreement with expected CARS concentration dependence and was used as a calibration for experiments in a flame. The scaling of the signal with pressure also revealed transition line-broadening effects up to 11 bar. The pressure effects were apparent, i.e., as low as 3 bar, but the signal increased with pressure-dependent number density up to 8 bar, above which it remained constant. Furthermore, application of the technique to a premixed dimethyl ether/air McKenna flat flame burner

yielded a similar trend to that shown in the previous literature, allowing additional characterization of the CH_2O concentration of this flame at varying heights and equivalence ratios with a precision of 11% or better. This was the first application of ERE-CARS measurements for CH_2O concentration, and the first application of a CARS technique to measure CH_2O concentration in a flame and in a high-pressure environment.

Funding. Air Force Research Laboratory (FA8650-19-F-2049).

Acknowledgment. We thank V. Athmanathan of Purdue University for technical assistance in the experiments.

Disclosures. The authors declare no conflict of interest.

REFERENCES

1. A. Perosa, M. Selva, V. Lucchini, M. Fabris, and M. Noè, "Kinetic parameter estimation of solvent-free reactions monitored by ^{13}C NMR spectroscopy, a case study: mono- and di-(hydroxy)ethylation of aniline with ethylene carbonate," Int. J. Chem. Kinet. **43**, 154–160 (2011).
2. J. Vandooren, L. O. de Guertechin, and P. J. Van Tiggelen, "Kinetics in a lean formaldehyde flame," Combust. Flame **64**, 127–139 (1986).
3. E. C. Tuazon, A. M. Winer, and J. N. Pitts, "Trace pollutant concentrations in a multiday smog episode in the California south coast air basin by long path length Fourier transform infrared spectroscopy," Environ. Sci. Technol. **15**, 1232–1237 (1981).
4. A. Rodriguez, O. Frottier, O. Herbinet, R. Fournet, R. Bounaceur, C. Fittschen, and F. Battin-Leclerc, "Experimental and modeling investigation of the low-temperature oxidation of dimethyl ether," J. Phys. Chem. A **119**, 7905–7923 (2015).
5. C. A. Idicheria and L. M. Pickett, "Formaldehyde visualization near lift-off location in a diesel jet," SAE Technical Paper 2006-01-3434 (2006).
6. K. Cung, X. Zhu, A. A. Moiz, S. Y. Lee, and W. De Ojeda, "Characteristics of formaldehyde (CH_2O) formation in dimethyl ether (DME) spray combustion using PLIF imaging," SAE Int. J. Fuels Lubr. **9**, 138–148 (2016).
7. J. Wang, M. Chaos, B. Yang, T. A. Cool, F. L. Dryer, T. Kasper, N. Hansen, P. Oßwald, K. Kohse-Höinghaus, and P. R. Westmoreland, "Composition of reaction intermediates for stoichiometric and fuel-rich dimethyl ether flames: flame-sampling mass spectrometry and modeling studies," Phys. Chem. Chem. Phys. **11**, 1328–1339 (2009).
8. A. Gratien, B. Picquet-Varrault, J. Orphal, E. Perraudin, J. F. Doussin, and J. M. Flaud, "Laboratory intercomparison of the formaldehyde absorption cross sections in the infrared (1660–1820 cm^{-1}) and ultraviolet (300–360 nm) spectral regions," J. Geophys. Res. Atmos. **112**, 1–10 (2007).
9. D. M. Smith, "Vibration-rotation interactions between overtone and combination levels of asymmetric-top molecules: application to the infrared spectroscopy of formaldehyde and ketene," J. Chem. Phys. **122**, 034307 (2005).
10. C. Ernest, "High-resolution studies of the $\tilde{A}^1A_2$–X^1A_1 electronic transition of formaldehyde: spectroscopy and photochemistry," Ph.D. Dissertation (University of Miami, 2017).
11. D. C. Moule and A. D. Walsh, "Ultraviolet spectra and excited states of formaldehyde," Chem. Rev. **75**, 67–84 (1975).
12. A. M. Walser, M. Meisinger, P. P. Radi, T. Gerber, and G. Knopp, "Resonant UV-fs-TCFWM spectroscopy on formaldehyde," Phys. Chem. Chem. Phys. **11**, 8456–8466 (2009).
13. E. W. Kaiser, T. J. Wallington, M. D. Hurley, J. Platz, H. J. Curran, W. J. Pitz, and C. K. Westbrook, "Experimental and modeling study of premixed atmospheric-pressure dimethyl ether–air flames," J. Phys. Chem. A **104**, 8194–8206 (2000).
14. J. B. Michael, P. Venkateswaran, J. D. Miller, M. N. Slipchenko, J. R. Gord, S. Roy, and T. R. Meyer, "100 kHz thousand-frame burst-mode imaging in turbulent flames," Opt. Lett. **39**, 739–742 (2014).
15. K. N. Gabet, R. A. Patton, N. Jiang, W. R. Lempert, and J. A. Sutton, "High-speed CH_2O PLIF imaging in turbulent flames using a pulse-burst laser system," Appl. Phys. B **106**, 569–575 (2012).
16. U. Retzer, R. Pan, T. Werblinski, F. J. T. Huber, M. N. Slipchenko, T. R. Meyer, L. Zigan, and S. Will, "Burst-mode OH/CH_2O planar laser-induced fluorescence imaging of the heat release zone in an unsteady flame," Opt. Express **26**, 18105–18114 (2018).
17. Z. Wang, P. Stamatoglou, M. Lundgren, L. Luise, B. M. Vaglieco, A. Andersson, M. Aldén, Ö. Andersson, and M. Richter, "Simultaneous 36 kHz PLIF/chemiluminescence imaging of fuel, CH_2O and combustion in a PPC engine," Proc. Combust. Inst. **37**, 4751–4758 (2019).
18. Z. Wang, P. Stamatoglou, Z. Li, M. Aldén, and M. Richter, "Ultra-high-speed PLIF imaging for simultaneous visualization of multiple species in turbulent flames," Opt. Express **25**, 30214–30228 (2017).
19. C. A. Fugger, S. Roy, A. W. Caswell, B. A. Rankin, and J. R. Gord, "Structure and dynamics of CH_2O, OH, and the velocity field of a confined bluff-body premixed flame, using simultaneous PLIF and PIV at 10kHz," Proc. Combust. Inst. **37**, 1461–1469 (2019).
20. S. A. Skeen, J. Manin, and L. M. Pickett, "Simultaneous formaldehyde PLIF and high-speed schlieren imaging for ignition visualization in high-pressure spray flames," Proc. Combust. Inst. **35**, 3167–3174 (2015).
21. K. Y. Cho, C. A. Fugger, R. T. Fievisohn, B. C. Sell, J. L. Hoke, S. P. Kearney, A. W. Caswell, J. R. Gord, and F. R. Schauer, "Burst-mode 355 nm plif for detonation wave front visualization and 100–300 kHZ particle image velocimetry," in *AIAA Scitech 2019 Forum* (2019), pp. 1–13.
22. J. D. Miller, S. J. Peltier, M. N. Slipchenko, J. G. Mance, T. M. Ombrello, J. R. Gord, and C. D. Carter, "Investigation of transient ignition processes in a model scramjet pilot cavity using simultaneous 100 kHz formaldehyde planar laser-induced fluorescence and CH* chemiluminescence imaging," Proc. Combust. Inst. **36**, 2865–2872 (2017).
23. S. Roy, J. R. Gord, and A. K. Patnaik, "Recent advances in coherent anti-Stokes Raman scattering spectroscopy: fundamental developments and applications in reacting flows," Prog. Energy Combust. Sci. **36**, 280–306 (2010).
24. A. M. Walser, P. Beaud, P. P. Radi, M. Tulej, T. Gerber, and G. Knopp, "Time-resolved investigation of the v_1 ro-vibrational Raman band of H_2CO with fs-CARS," J. Raman Spectrosc. **38**, 1538–1553 (2007).
25. B. Attal, D. Débarre, K. Müller-Dethlefs, and J. P. E. Taran, "Resonance-enhanced coherent anti-Stokes Raman scattering in C_2," Rev. Phys. Appl. **18**, 39–50 (1983).
26. S. F. Hanna, W. D. Kulatilaka, Z. Arp, T. Opatrný, M. O. Scully, J. P. Kuehner, and R. P. Lucht, "Electronic-resonance-enhanced coherent anti-Stokes Raman spectroscopy of nitric oxide," Appl. Phys. Lett. **83**, 1887–1889 (2003).
27. W. D. Kulatilaka, N. Chai, S. V. Naik, N. M. Laurendeau, R. P. Lucht, J. P. Kuehner, S. Roy, and J. R. Gord, "Measurement of nitric oxide concentrations in flames by using electronic-resonance-enhanced coherent anti-Stokes Raman scattering," Opt. Lett. **31**, 3357–3359 (2006).
28. B. Attal-Trétout, P. Berlemont, and J. P. Taran, "Three-colour CARS spectroscopy of the OH radical at triple resonance," Mol. Phys. **70**, 1–51 (1990).
29. P. J. Wrzesinski, H. U. Stauffer, J. B. Schmidt, S. Roy, and J. R. Gord, "Femtosecond fully resonant electronically enhanced CARS (FREE-CARS) for simultaneous minor-species detection and single-shot thermometry," Opt. Lett. **41**, 2021–2024 (2016).
30. N. Chai, W. D. Kulatilaka, S. V. Naik, N. M. Laurendeau, R. P. Lucht, J. P. Kuehner, S. Roy, V. R. Katta, and J. R. Gord, "Nitric oxide concentration measurements in atmospheric pressure flames using electronic-resonance-enhanced coherent anti-Stokes Raman scattering," Appl. Phys. B **88**, 141–150 (2007).
31. J. A. Shirley, R. J. Hall, and A. C. Eckbreth, "Folded BOXCARS for rotational Raman studies," Opt. Lett. **5**, 380–382 (1980).
32. A. M. Walser, "Time-resolved four-wave mixing spectroscopy of gaseous formaldehyde," Ph.D. Dissertation (ETH Zurich, 2008).
33. M. Tulej, M. Meisinger, G. Knopp, A. M. Walser, P. Beaud, T. Gerber, and P. P. Radi, "Degenerate and two-color resonant four-wave mixing applied to the rotational characterization of high-lying vibrational states of formaldehyde ($\tilde{A}$, $^1A_2$)," J. Raman Spectrosc. **37**, 376–383 (2006).

34. D. J. Clouthier and D. A. Ramsay, "The spectroscopy of formaldehyde and thioformaldehyde," Annu. Rev. Phys. Chem. **34**, 31–58 (1983).
35. R. J. Bouwens, J. A. Hammerschmidt, M. M. Grzeskowiak, T. A. Stegink, P. M. Yorba, and W. F. Polik, "Pure vibrational spectroscopy of S0 formaldehyde by dispersed fluorescence," J. Chem. Phys. **104**, 460–479 (1996).
36. G. Magnotti, K. C. Utsav, P. L. Varghese, and R. S. Barlow, "Raman spectra of methane, ethylene, ethane, dimethyl ether, formaldehyde and propane for combustion applications," J. Quant. Spectrosc. Radiat. Transf. **163**, 80–101 (2015).
37. P. R. Régnier and J. P. E. Taran, "On the possibility of measuring gas concentrations by stimulated anti-Stokes scattering," Appl. Phys. Lett. **23**, 240–242 (1973).
38. W. D. Kulatilaka, N. Chai, S. V. Naik, S. Roy, N. M. Laurendeau, R. P. Lucht, J. P. Kuehner, and J. R. Gord, "Effects of pressure variations on electronic-resonance-enhanced coherent anti-Stokes Raman scattering of nitric oxide," Opt. Commun. **274**, 441–446 (2007).
39. K. A. Rahman, V. Athmanathan, M. N. Slipchenko, T. R. Meyer, and S. Roy, "Pressure-scaling characteristics of femtosecond two-photon laser-induced fluorescence of carbon monoxide," Appl. Opt. **58**, 7458–7465 (2019).